Research article

X-RAY SPECTROMETRY

Received: 9 June 2016 Revised: 19 September 2016 Accepted: 3 October 2016 Published online in Wiley Online Library: 7 November 2016

(wileyonlinelibrary.com) DOI 10.1002/xrs.2723

Characterization of biomaterials commonly used in dentistry for bone augmentation by X-ray and electron techniques

S. Limandri,[a]* S. P. Fernandez Bordín,[a] M. Gersberg,[b] L. Brito,[b] R. G. Oliveira,[c] G. Fouga[d] and V. Galván Josa[a]

Hydroxyapatite (HA), beta-tricalcium phosphate and bioactive glasses are commonly used as reabsorbable biomaterials, mainly in orthopaedics and dentistry. The performance of each material depends on many factors, in particular, on their chemical and phase composition, microstructure, granule size and pore volume. For this reason, it is important to have a full characterization that allows correlating these properties with the material biological behaviour.

In this work, three commercial samples of materials currently used in dentistry as bone substitutes were characterized. Granules corresponding to bovine and synthetic HA and bioactive glass 45S5 type were studied by scanning electron microscopy, conventional and synchrotron radiation X-ray diffraction and X-ray fluorescence. The specific surface area was also obtained by the Brunauer, Emmett and Teller method.

We observed that Ca/P molar ratios for both HAs are higher than the value corresponding to the stoichiometric HA. The coherent domain obtained for the bovine HA is larger along the *c* axis crystal direction, and it is around 15 times lower than the value corresponding to the synthetic HA. The specific surface area for the bovine HA is one of the highest values reported in literature. Low amounts of crystalline CaO were observed only for the synthetic HA sample. Crystalline combeite and wollastonite were detected for the bioactive glass sample and quantified by using rutile as internal standard. The relation between the physicochemical characterization performed in this work and the potential biological response of the materials is discussed in terms of the information available in literature. Copyright © 2016 John Wiley & Sons, Ltd.

Introduction

Tissue engineering is an interdisciplinary field in which engineering and life science principles are combined to obtain biological substitutes capable of restoring, keeping or improving the function of the tissue or organ that has been affected. The success of this approach partially depends on the development of porous matrices or scaffolds able to provide the cell support necessary for proliferation and maintenance of the functions (or biological signals) required for the conservation of the specific gene expression in the tissue.

To be accepted as a bone matrix, a material must fulfil certain requirements related to biocompatibility, osteoconduction, osseointegration and bioabsorbability and it must have suitable mechanical properties to provide a structural support during bone growth.[1] Several *in vivo* and *in vitro* experiments have shown that calcium phosphates in many forms (porous blocks, surface coatings and powders, among others) and phases (crystalline and amorphous) support the attachment, differentiation and proliferation of cells (such as osteoblasts and mesenchymal cells). Two types of orthophosphoric acid salt, known as beta-tricalcium phosphate (TCP) and hydroxyapatite (HA), are commonly used as reabsorbable biomaterials.[2]

Hydroxyapatite, $Ca_5(PO_4)_3(OH)$, is one of the few materials classified as bioactive, i.e. as a material that support bone growth and osseointegration when used in orthopaedic, dental and maxillofacial applications. These properties are related to the similarity between HA and the inorganic bone components.[2] HA coatings are often used in metallic implants (particularly in stainless steel and titanium alloy-based implants) to improve surface properties. In addition, HA is used in all its forms as a filler material for bone restoration. Besides medical applications, HA is implemented in many fields such as catalysis, gas sensors and gas chromatography.[3]

Several studies suggest that many properties of HA are affected by its particular chemical composition. For instance, bioactivity and osteoconduction are associated with material solubility, which decreases when OH is replaced by F[4] and increases when some Ca atoms are substituted by Sr.[5,6] Bone strength is inversely

* *Correspondence to: S. Limandri, Instituto de Física Enrique Gaviola, Facultad de Matemática, Astronomía y Física, CONICET, Medina Allende s/n, Ciudad Universitaria, X5000HUA Córdoba, Argentina. E-mail: limandri@famaf.unc.edu.ar*

a *Instituto de Física Enrique Gaviola, Facultad de Matemática, Astronomía y Física, CONICET, Medina Allende s/n, Ciudad Universitaria, X5000HUA, Córdoba, Argentina*

b *ODONTIT Argentina S.A., Azcuénaga 1077, Buenos Aires, Argentina*

c *Centro de Investigaciones en Química Biológica de Córdoba, CIQUIBIC, CONICET, Departamento de Química Biológica, Facultad de Ciencias Químicas, Universidad Nacional de Córdoba, Medina Allende y Haya de la Torre, Ciudad Universitaria, X5000HUA, Córdoba, Argentina*

d *Departamento de Fisicoquímica y Control de Calidad, Complejo Tecnológico Pilcaniyeu, Centro Atómico Bariloche, Comisión Nacional de Energía Atómica, CONICET, Av. Bustillo 9500, 8400, S.C. de Bariloche, Río Negro, Argentina*

proportional to the crystal size,[7] which decreases for higher Sr concentrations.[5] The Ca/P molar fraction is related to the mechanical properties of HA (Young modulus, hardness and fracture toughness). According to Ramesh *et al.*,[8] if HA satisfies the stoichiometric Ca/P relation, then the global mechanical properties are better than the ones corresponding to non-stoichiometric HA.

Although different methods can be applied to synthesize HA,[9] the most widely used is the precipitation method. Synthetic HA is one of the most efficient calcium phosphates due to its stability against changes in pH, temperature and physiological fluid composition. In general, it is highly pure, and the Ca/P molar ratio, grain size, porosity and crystallinity can be controlled during the synthesis. Nevertheless, some synthesis processes are complicated and/or biologically hazardous. For these reasons, obtaining HA from natural sources is usually considered.[10] Natural sources are, in addition, economically and environmentally preferable. Some biowastes such as animal bones and teeth, corals, egg shells and agrowastes have been used to obtain HA.[2,11–14]

A great variety of bioactive glasses have been investigated for bone restoration and are applied successfully nowadays in many clinical applications.[15] The fast bioactive behaviour of silica-based glasses has been related to the role of SiO_2 or silicon in reactions occurring at the surface. The surface of an implanted bioactive glass transforms into a gel layer when it is immersed in a solution or body fluid, which subsequently mineralizes, forming a carbonated substituted HA-like layer.[15] The gel layer resembles the HA matrix and facilitates the new bone growth.

As it was stated before, the performance of each material depends on its mechanical, structural, topographic and chemical properties. For this reason, it is important to have a full characterization that allows correlating these properties with the material biological behaviour. Several techniques have been used to characterize biomaterials and apatites, for instance, X-ray microdiffraction,[16] scanning electron microscopy (SEM)[17] and X-ray fluorescence (XRF),[18] among others.

In this work, chemical and surface properties are studied for commercial synthetic and bovine HAs and bioactive glass 45S5 type applied in dentistry. Phase purity is characterized by X-ray diffraction (XRD) and XRF techniques. Morphological characterization is performed by SEM, and the specific surface area is determined by the Brunauer, Emmett and Teller (BET) method. The relation between the physico-chemical properties and the biological material response is discussed in terms of the information available in the literature.

Materials and methods

Samples

The studied samples were provided by ODONTIT Argentina S.A. and correspond to commercial powders. These materials are used for the treatment of bone defects and bone augmentation, reconstruction and increase of alveolar ridge, filling post extraction alveoli, preparation of site implants, filling of osseous dehiscence, maxillary sinusal elevation and filling osseous defects in tissue-guided regeneration. A brief description of the synthesis methods and specifications given by the manufacturer is given in the succeeding texts.

Synthetic HA

The synthetic powder SYNERGY® is obtained by the precipitation method. According to the manufacturer, synthesis and purification processes are followed from pure reactives (>99%) to obtain this material. Calcium nitrate, $Ca(NO_3)_2(H_2O)$; ammonium phosphate, $H_2(PO_4)NH_4$; and ammonium hydroxide, NH_4OH, are used to complete the following chemical reaction at 1200 °C:

$$10\,Ca(NO_3)_2 + 6\,(NH_4)_2HPO_4 + 8\,NH_4OH \rightarrow Ca_{10}(PO_4)_6(OH)_2 + 20\,NH_4NO_3 + 6\,H_2O \quad (1)$$

Bovine HA

The bovine HA powder SYNERGY® is obtained from spongy bovine bones by calcination process at 500 °C.

Bioactive glass

High-purity silica and reagent-grade calcium carbonate, sodium carbonate and phosphorous pentoxide are weighted and mixed to obtain a final product with a nominal composition of 45 wt% SiO_2, 24.5 wt% CaO, 24.5 wt% Na_2O and 6.0 wt% P_2O_5 (45S5 type glass). The mixture is melted in a Pt crucible for 4 h at 1330 °C and then quenched in water.

Techniques

Scanning electron microscopy

The powders as received were dispersed in a carbon tape and covered by a 10-nm-thin gold layer. The microstructure was observed from secondary electron images, acquired in a field emission SEM Σigma Zeiss electron microscope and operated at 5 kV. Low magnification images [Figs 1(a) and (b) and 3(a) and (b)] were acquired with a conventional Everhart–Thornley secondary electron detector, whereas the high magnification images [Figs 1(c) and (d) and 3(c) and (d)] were obtained with an in-lens secondary detector. The Oxford energy dispersive silicon drift detector X-ray detector attached to the equipment, with 80-mm^2 front area and nominal resolution of 127 eV for Mn-Kα line, was used to identify the chemical composition of minor phases for the bioactive glass sample.

X-ray fluorescence

Three fusion beads for each sample type were prepared in order to obtain reproducible results with a Claisse M4 FLUX-lite tetraborate–dilithiumtetraborate (Claisse, Canada). For each pearl, 1 g of sample and 8 g of flux were weighed (with an accuracy of 0.0001 g) and put into a previously cleaned crucible. The advantages of using pearls against the conventional press pellets are the removement of the heterogeneity, substantial decrease of interelement influence and lower consumption of sample, which leads to a high reliability of results.

Measurements were performed in an XRF sequential spectrometer Bruker F8 Tiger. The X-ray tube has an Rh anode, and the characteristic X-ray lines were detected with LiF(200) (K–U), PET (Al–Cl) and XS-55 (O–Mg) crystals coupled with a proportional counter (for low Z elements) and a scintillator counter (for high Z elements).

X-ray diffraction

X-ray diffraction measurements for HA powders were carried out at the XRD-1 beamline, LNLS, Brazil. Samples were measured in transmission geometry by using a collimated X-ray beam with a primary energy of 12 keV. The patterns were collected in the interval of 2.7°–120.7° 2θ with 0.004° steps by using an array of 24 Mythen detectors placed in the delta circle at a distance of 76 cm from the sample. Initial calibration of the diffraction setup was performed by using a silicon standard reference sample (NIST 640d).

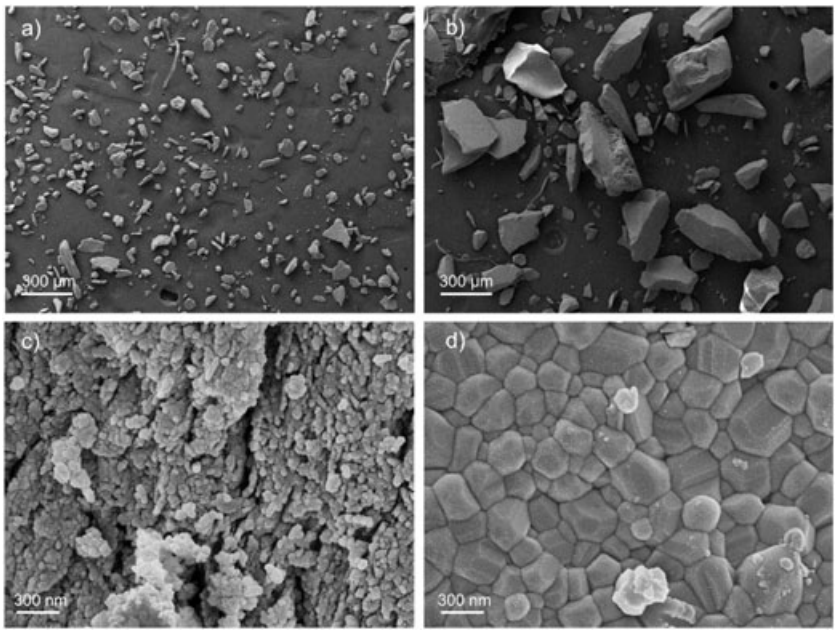

Figure 1. Secondary electron micrographs corresponding to bovine (a and c) and synthetic (b and d) HA samples.

The X-ray diffractograms of the bioglass sample were obtained with a Panalytical Empyrean X-ray diffractometer, with voltage and current settings of 40 kV and 40 mA respectively, and Cu-Kα radiation. The XRD patterns were recorded in the interval of 5°–90° 2θ with a step size of 0.02°.

Rietveld refinements with DIFFRACPLUS TOPAS® software were performed in order to quantify the crystalline phases for all the studied samples. The parameters refined for the HA samples were the background, which was modelled by sixth-order Chebyshev polynomial; the zero correction; scale factors; temperature factors; the crystallite size and some occupancy factors of HA. The Inorganic Crystal Structure Database code used as starting crystallographic data for HA was #22059.

The quantification of the amorphous and crystalline content for the bioactive glass sample was performed by adding 20 wt% of rutile (TiO_2), which was used as internal standard.

Surface area

The specific surface areas were determined by the triple-point BET method,[19] with nitrogen or kripton as adsorbate gases. The samples were dried and degassed at 400 °C for 2 h. Measurements were carried out in a DigiSorb 2600 Micromeritics surface area analyser. Nitrogen was used as adsorbate gas for the bovine HA sample, whereas krypton gas was used for synthetic HA and bioactive glass.

Results and discussion

Bovine HA particles are mainly oblong with rounded edges [Fig. 1(a)]. According to the statistical study performed on 400 particles, the particle size ranges between 1 and 370 µm with a mean diameter of 40 µm (Fig. 2). Only 2% of the analysed particles present diameters higher than 150 µm. Nevertheless, this fraction represent the 62% of mass analysed. The particle structure consists of an agglomerate of nanosized highly porous grains [Fig. 1(c)]. The mean diameter of these subunits, obtained by performing 100 individual measurements on the high magnification images,

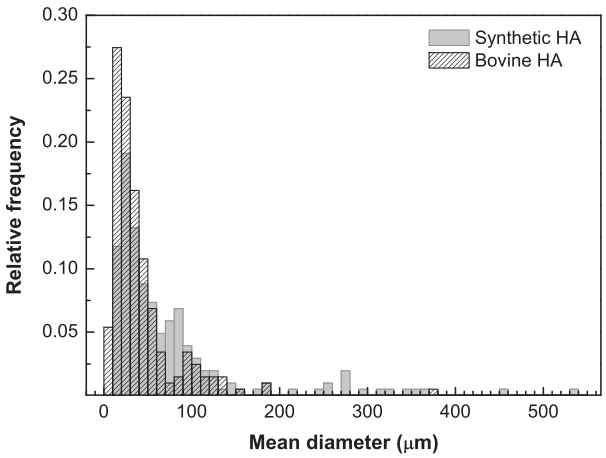

Figure 2. Particle diameter distribution obtained from the SEM images for the HA samples.

resulted in 42 ± 7 nm, and their irregular morphology indicates that they are not completely coherent crystalline domains. The presence of nanopores is related with better resorbability and bioactivity properties.[20]

Synthetic HA particles have a wider range of sizes and shapes [Fig. 1(b)]. The statistical analysis perfomed on 400 particles shows that the particle diameter ranges between 10 and 550 µm. The corresponding distribution has apparently maximums at 30, 90 and 280 µm (Fig. 2). To clearly define these maximums with sufficient statistical significance, more measurements should be performed. Particles with diameter higher than 150 µm (which corresponds to 10% of the total number of sampled particles) contain 90% of the mass analysed. Fine grains with crystalline facets stuck together (associated with low nanoporosity) can be observed in the images acquired at high magnification [Fig. 1(d)]. Nanocrystals have polyhedric shapes with a mean grain diameter of 210 ± 30 nm. According to the micrographs, the porosity of synthetic particles is lower than that corresponding to the bovine ones.

The particles corresponding to the bioactive glass sample present a wide dispersion of sizes (with diameters ranging from 1 to 400 μm); they are composed mainly of vitreous aggregates, and the larger ones have sharp-edge shards (Fig. 3). The presence of rod-like structures corresponding to a crystalline phase can be observed in Fig. 3(c). According to the corresponding characteristic X-ray spectrum, these rods have a higher Na content than that corresponding to the amorphous matrix and can be associated with the combeite phase ($Na_2Ca_2Si_3O_9$), detected by XRD (see succeeding texts). The mean rod length and width are 3.9 ± 1.5 and 0.8 ± 0.2 μm respectively. Some of the largest particles present circular holes with a diameter of around 70 μm [Fig. 3(b)] due to the carbon dioxide released in the melt-quenching process. The inner hole region is rougher than the particle surface.

Mass oxide concentrations obtained by XRF are shown in Table 1. Our results for major elements are in good agreement with data reported by other authors for bovine HAs.[10,21] For this sample, comparing with synthetic HA, higher amounts of Mg and Sr and other minor elements (Na, K, Fe and Zn) were detected. The presence of trace elements is expected for HA obtained from natural sources because the ionic components in HA [Ca^{2+}, OH^- and $(PO_4)_3$] can be interchanged by other ions,[20] in particular, some Ca sites are usually substituted by Sr and Mg in natural bone. In addition, the type and amount of trace elements depend on the bone type used as raw material and on some biological factors (such as animal nutrition).[10,22]

Molar Ca/P ratios are higher than the stoichiometric value (1.67) for the studied HAs. According to Miecznik *et al.*,[23] this deviation is expectable for bovine HA, whereas for synthetic samples, the molar ratio depends on the sintering temperature and chemical precursors used. Wang *et al.* showed that apatites with higher/lower molar relations (relative to the stoichiometric value) are prone to present crystalline CaO/beta-TCP respectively. [24] In addition, they stated that the presence of TCP is less prejudicial than that of crystalline CaO. Crystalline calcium oxide amounts higher than 1% render the bulk ceramic more susceptible to degradation because CaO increases the rate of intergranular corrosion by weakening the grain boundaries and serve as a potent trigger for media-based precipitation.[24] In this work, low amounts of crystalline CaO were detected by XRD only for the synthetic HA (see succeeding texts).

The chemical composition corresponding to the bioactive glass sample is similar to the nominal composition of 45S5 glass. The molar Ca/P ratio obtained for this sample is higher than 5, which is advantageous because the glass does not bind to bone if the ratio is lower than this value.[25] The trace elements found for this

Table 1. Oxide mass concentrations obtained by XRF for the studied samples

	wt% oxide concentration		
Oxide	Synthetic HA	Bovine HA	Bioactive Glass
Na_2O		1.61	27.31
MgO	0.25	1.53	0.24
Al_2O_3			0.73
SiO_2	0.23		46.2
P_2O_5	41.83	38.54	4.1
SO_3	0.16	0.02	0.03
Cl			0.07
K_2O		0.01	0.09
CaO	57.52	58.18	21.12
TiO_2			0.03
Fe_2O_3		0.01	0.06
NiO			0.003
ZnO		0.02	
SrO	0.008	0.07	0.01
ZrO_2			0.01
Ca/P molar ratio	1.74	1.91	6.52

The results correspond to the mean values of three independent measurements performed for each sample. The estimated errors are in the last digit.

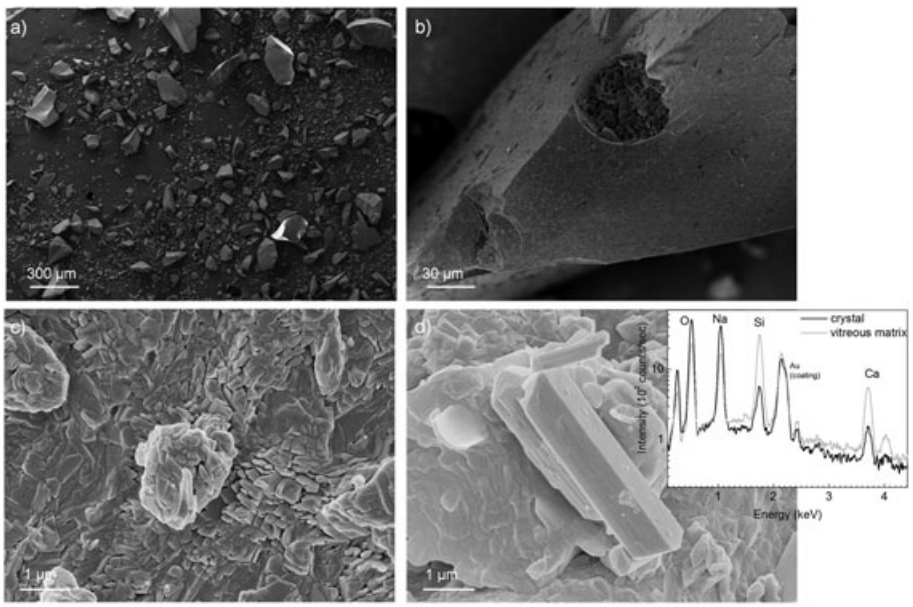

Figure 3. Secondary electron micrographs corresponding to bioactive glass particles. (a) General view, (b) large particle, (c) amorphous matrix and (d) rod-like crystal. The inset corresponds to energy-dispersive characteristic X-ray spectra acquired for the amorphous matrix and the rod-like crystal.

sample are associated with the impurities of the reactives used in the synthesis process. The presence of Sr is considered as beneficial because it promotes a better bone bonding.[26] On the other hand, TiO_2 and Al_2O_3 impurities negatively affect solubility properties and mineralization processes of the bioactive glass. Mass concentrations higher than 1% and 7% for TiO_2 and Al_2O_3 respectively, extend the time necessary to achieve the material–bone connection.[27] Even when the amounts of TiO_2 and Al_2O_3 determined in this work are lower than these values, it would be recommended to use higher purity precursors in the bioactive glass formulation.

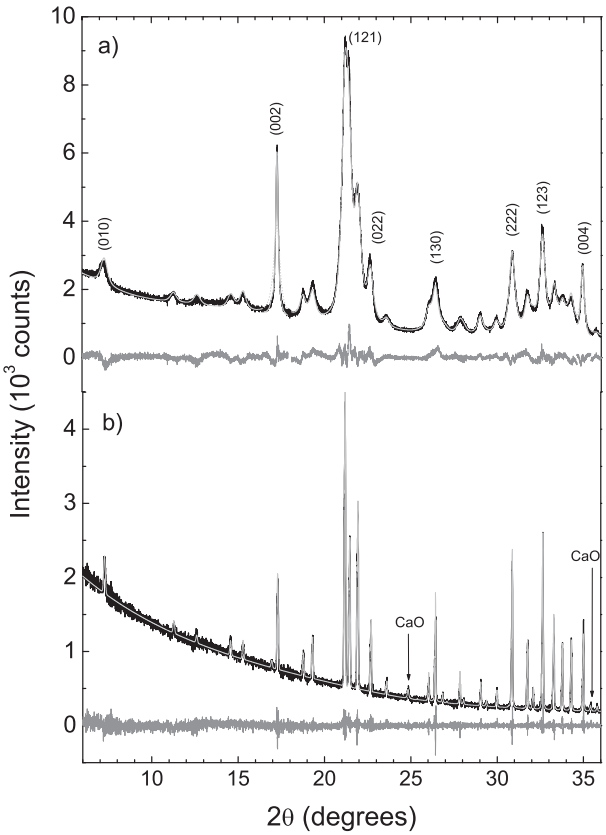

Figure 4. Synchrotron radiation XRD patterns and Rietveld refinement corresponding to (a) bovine and (b) synthetic HAs. Black line: experimental; light grey solid line: final fit (see text); grey line: residue; light grey dotted line: fit corresponding to {001} reflections by using the average crystallite size value (11 nm); CaO: crystalline calcium oxide.

The synchrotron radiation XRD patterns corresponding to the studied HAs are shown in Fig. 4. The peaks associated with HA phase are sharper for the synthetic sample. The lower diffraction intensity for natural extracted HA compared with synthetic HA is related to the presence of a higher amount of disordered phase (low crystallinity phase) in the bovine HA sample.[28] The fits are acceptable for both patterns, as can be seen in the goodness-of-fit factors (Table 2). The lattice parameters obtained for the bovine and synthetic HA samples are, respectively, $a = b = 9.414$ Å, $c = 6.892$ Å and $a = b = 9.403$ Å, $c = 6.867$ Å.

For bovine HA, the peaks associated with 002 and 004 reflections are narrower than the ones predicted by fitting the complete 2θ region. This is related to an anisotropy effect in the crystallite size. For this reason, the fitting was perfomed in two regions: one excluding the {001} reflections and other exclusively containing the {001} reflections. The corresponding crystallite sizes are 11 and 23 nm for each considered region respectively, which means that the coherent domain along the *c* axis direction is around two times higher than the size in *a* direction. This behaviour is expected for HAs obtained from bones because in natural bone apatite crystals nucleate on and grow within the collagen network acquiring a plate-shape form, with the *c* axis parallel to the long axis of the microfibril.[20,29] Pramanik *et al.*[30] observed a similar trend for bovine HA treated at 1200 °C for 2 h, although the ratio between the sizes in the perpendicular and parallel to *c* directions resulted barely higher than 1. The high sintering temperature used by these authors allowed grain growth, decreasing the crystal anisotropy effect.

The small crystal domains obtained for bovine HA will result in a major contact reaction and stability in the interphase with natural bone when implanted, and it will have a better promotion effect on the early bone in-growth.[31] Crystallite sizes determined for several authors for bovine HAs under different heat treatment temperatures are shown in Fig. 5. As can be seen, the crystalline domains are higher when the sintering temperature increases. The great dispersion of data for higher temperatures could be related to the different sintering times and steps used by different authors: Madhavi *et al.*[32] performed the synthesis by maintaining samples at 400 °C for 3 h (at a heating rate of 1 °C/min), and then the calcination was performed at the final temperature for 1 h (with a heating rate of 2 °C/min); Bahrololoom *et al.*[10] and Pramanik *et al.*[33] used a heat treatment time of 3 h. The last authors used a two-step sintering method. Besides the heat treatment steps, there are some chemical factors that also affect the final crystallite size;

Table 2. Quantitative results obtained by XRD for the HAs and bioactive glass samples

		Synthetic HA	Bovine HA	Bioactive Glass
wt% phase concentration	Hydroxyapatite $Ca_5(PO_4)_3(OH)$	99.3	100	
	Calcium oxide (CaO)	0.7		
	Combeite ($Na_2Ca_2Si_3O_9$)			4.0
	Wollastonite ($CaSiO_3$)			0.3
	Amorphous			95.7
	Average crystallite size (nm)	170	11	
	Crystallite size ratio (002)/(200)	1.1	2.1	
	Goodness of fit	1.4	1.7	2.2

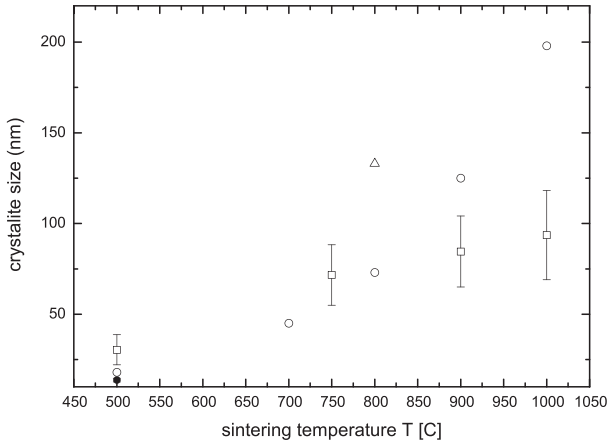

Figure 5. Crystallite size as a function of the heat treatment temperature for HAs obtained from natural sources. Black circle: this work; triangle: Bahrololoom *et al.*[10]; squares: mean value corresponding to distal, middle and proximal bovine femurs obtained by Pramanik *et al.*[33]; white circles: Madhavi *et al.*[32]

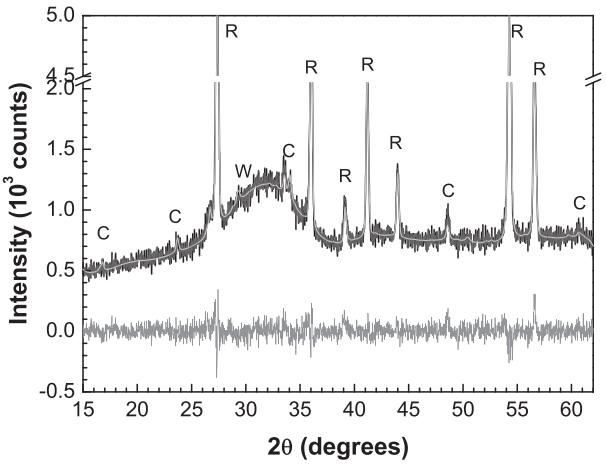

Figure 6. XRD pattern and Rietveld refinement corresponding to the bioactive glass sample with 20 wt% rutile as internal standard. R, rutile (TiO2); C, combeite (Na2Ca2Si3O9); W, wollastonite (CaSiO3); black, experimental; light grey, fit; grey, residue.

these include denaturing of the bone matrix during burning through release of water, in which the mineral crystals recrystallize, and removal of the collagen fibril networks which influence the crystallite size of the bone ash.[10]

Recrystallization processes without transformation into another calcium phosphate phase begin around 600 °C in bovine HA.[10] For the bovine HA sample studied in this work, the sintering temperature is lower than this value, so phase recrystallization is not expected. Keeping the natural small crystalline domains could be advantageous because bone strength is inversely proportional to the crystal size.[7]

From the Rietveld refinement, we obtained that 5% of the Ca(1) site is occupied by Mg atoms in the studied bovine HA sample, which implies a presence of around 1 wt% of Mg. This value is in good agreement with the results obtained by XRF. For synthetic HA, the Ca substitution by Mg can be inferred only from XRF measurements.

As it was mentioned in the preceding texts, several authors have shown that free calcium oxide constitutes a very undesirable impurity of the HA ceramics, and in general, it excludes the possibility to use such material in biological applications.[24,34] We did not detect free crystalline calcium oxide in bovine HA, whereas the amount detected for synthetic HA is lower than 1% (Table 2). This value does not affect the biocompatibility of this material.[24]

The bioactive glass sample is mainly amorphous and presents combeite and wollastonite crystalline minor phases (Fig. 6). The amount of these crystalline phases could be reduced by decreasing the sintering temperature or by using liquid nitrogen in the quenching process. The studies performed by Rahaman *et al.*[15] and Rizkalla *et al.*[35] show that several bioactive glasses crystallize as combeite and wollastonite. The presence of combeite does not inhibit the glass ability to form an HA-like surface layer, but it has the effect of reducing the rate of conversion into HA.[36] Despite this negative effect, the partial crystallization of bioactive glasses increases their chemical durability, density, microhardness and flexural strength.[37] The presence of wollastonite does not affect the glass biocompatibility. On the contrary, Sautier *et al.*[38] and Kitsugi *et al.*[39] showed that for glass–ceramics composed of bioactive glass + wollastonite + apatite, the crystalline phases can be beneficial for the initiation of biomineralization in osteoblasts, leading to achieve a direct bond between the surface apatite layer of the bioactive glass–ceramic and the mineralized bone matrix.

The specific surface areas obtained in this work for the studied HAs are 111.5 ± 0.6 and $<0.1\ m^2/g$ for bovine and synthetic materials respectively. The low value obtained for the synthetic sample agrees with the low porous structure and high particle sizes observed in the SEM images. The BET area corresponding to the bovine HA lies within the highest values reported in the literature. Figueiredo *et al.*[40] characterized commercial HAs obtained from several natural sources (bovine, porcine and coraline), obtaining BET areas in a large range: 59.7 and $1.72\ m^2/g$ for two bovine samples, $42.4\ m^2/g$ for porcine and $0.26\ m^2/g$ for coralline materials. The authors associate these differences to two factors: the sample surface characteristics and the particle size. Large BET area values are associated with a rough surface and with the type of bone used (cancellous bones lead to more porous material than cortical bones). In addition, high temperature treatments create large intraparticle pores, decreasing the BET area, so there is a compromise between the temperature used to achieve a complete calcination of the raw material and the desired final microstructure. The highest BET area for bovine HA corresponds to $223\ m^2/g$ and was obtained by Moreno-Pirajan *et al.*[41] by performing the charring in an inert atmosphere.

In the case of synthetic HA, the BET areas reported by other authors belong to a wide range and mainly depend on the production process. For instance, Ramli *et al.*[42] obtained a BET area of $24\ m^2/g$ by co-precipitation method (at 800 °C for 2 h), Sobczak-Kupieca *et al.*[43] measured $77.62\ m^2/g$ for samples obtained by wet method, Markovic *et al.*[44] reported a value of $18.3\ m^2/g$ for samples synthesized by reaction of calcium hydroxide and phosphoric acid, Lin *et al.*[45] obtained $17.3\ m^2/g$ by spark plasma sintering at 850 °C, and one of the highest values reported in the literature is $115.6\ m^2/g$ and was obtained by Ciobanu *et al.*[46] for europium-doped HA. All these values are higher than the one obtained in this work.

For the bioactive glass sample, the specific surface area is $0.79 \pm 0.01\ m^2/g$. Information available in literature for BET areas of bioactive glasses is lower than that corresponding to HAs. Several authors state that the largest BET area corresponds to bioactive glasses obtained by sol-gel technique.[47] Values between 0.15 and $2.7\ m^2/g$ were reported for melt-cast methods (being the larger

BET areas associated with the lower particle sizes), whereas the BET area is considerable higher than these values (around 165 m^2/g) for sol-gel methods.[48,49]

Conclusions

Three commercial samples of materials currently used in dentistry as bone substitutes were characterized by SEM and X-ray techniques. The specific surface area was also obtained by the BET method. By adequately applying these techniques, the chemical and mineralogical compositions of bioceramics and bioglass samples were satisfactorily obtained and compared with data available in the literature. The studied samples can be divided in two groups: one comprising the HA-based materials and the other constituted by the bioactive glass 45S5 type.

Even for the HAs that present similar chemical characteristics, significant differences were observed in terms of particle size, crystallinity, surface area and crystalline phase content. Bovine HA particles are oblong and present a very high BET area, whereas synthetic HA particles have sharp edges and crystalline grains stuck together with a very low porosity. The crystalline domains are also very different, being around 15 times higher for synthetic HA. Coherent crystalline domains for bovine HA are larger along the *c* axis direction. This was observed from the low ratio between the peak widths associated with the (002) planes relative to other diffraction peaks.

Bioactive glass is mainly amorphous but presents around 4% and 0.3% of combeite and wollastonite minerals respectively. The internal standard method in XRD was very useful not only to detect and identify minor crystalline phases in an amorphous matrix but also to quantify them. XRF measurements in fusion beads allowed as to detect and precisely quantify the minor and trace elements present in the studied samples, some of which could not be associated with mineral phases detected by XRD.

Acknowledgements

The authors gratefully acknowledge the Laboratorio de Microscopía Electrónica y Análisis por Técnicas de Rayos X (Argentina), the Centro Atómico Bariloche (Argentina) and the XRD-1 beamline at the Laboratório Nacional de Luz Síncrotron (Brazil), where measurements were carried out. Financial support from the Consejo Nacional de Investigaciones Científicas y Técnicas (Argentina) and the Secretaría de Ciencia y Técnica de la Universidad Nacional de Córdoba is also acknowledged.

References

[1] S. V. Dorozhkin. *J. Mater. Sci.* **2009**, *44*, 2343.
[2] J. R. Jones, L. L. Hench. *Mater. Sci. Tech.* **2001**, *17*, 891.
[3] M. Subramanian, G. Vanangamudi, G. Thirunarayanan. *Spectrochim. Acta, Part A* **2013**, *110*, 116.
[4] K. Cheng, G. Shen, W. Weng, G. Han, J. M. F. Ferreira, J. Yang. *Mater. Lett.* **2001**, *51*, 37.
[5] S. C. Verberckmoes, G. J. Behets, L. Oste, A. R. Bervoets, L. V. Lamberts, M. Drakopoulos, A. Somogyi, P. Cool, W. Dorriné, M. E. De Broe, P. C. D'Haese. *Calcif. Tissue Int.* **2004**, *75*, 405.
[6] L. Oste, S. Verbeckmoes, G. Behets, G. Dams, A. Bervoets, V. Van Hoof, S. Bohic, M. Drakopoulos, M. De Broe, P. D. `Haese. *X-Ray Spectrometry* **2007**, *36*, 42.
[7] E. P. Paschalis, F. Betts, E. DiCarlo, R. Mendelsohn, A. L. Boskey. *Calcif. Tissue Int.* **1997**, *61*, 487.
[8] S. Ramesh, C. Y. Tan, M. Hamdi, I. Sopyan, W. D. Teng. *Proc. SPIE* **2007**, *6423*, 64233A.
[9] M. Sadat-Shojai, M. Khorasani, E. Dinapanah-Khoshdargi, A. Jamshidi. *Acta Biomater.* **2013**, *9*, 7591.
[10] M. E. Bahrololoom, M. Javidi, S. Javadpour, J. Ma. *J. Ceram. Process. Res.* **2009**, *10*, 129.
[11] M. Ozawa, S. Suzuki. *J. Am. Ceram. Soc.* **2002**, *85*, 1315.
[12] U. Iriarte-Velasco, I. Sierra, L. Zudaire, J. Ayastuy. *J. Mater. Sci.* **2015**, *50*, 7568.
[13] S. C. Wua, H. C. Hsua, Y. N. Wu, W. F. Ho. *Mater Charact* **2011**, *62*, 1180.
[14] D. Gopi, K. Bhuvaneshwari, J. Indira, K. Louis. *Spectrochim. Acta, Part A* **2014**, *118*, 589.
[15] M. N. Rahaman, D. E. Day, B. S. Bal, Q. Fu, S. B. Jung, L. F. Bonewald, A. P. Tomsia. *Acta Biomater.* **2011**, *7*, 2355.
[16] B. A. Cedolaa, S. Lagomarsinoa, V. Komlevb, F. Rustichellib, M. Mastrogiacomoc, R. Canceddac, S. Militad, M. Burghammere. *Spectrochim. Acta, Part B* **2004**, *59*, 1557.
[17] G. Valdré. *X-Ray Spectrom.* **1994**, *23*, 120.
[18] M. Rabionet, J. Toque, A. Ide-Ektessabi. *X-Ray Spectrom.* **2009**, *38*, 278.
[19] S. Brunauer, P. H. Emmett, E. Teller. *J. Am. Chem. Soc.* **1938**, *60*, 309.
[20] M. Šupová. *Ceram. Int.* **2015**, *41*, 9203.
[21] K. Haberko, M. M. Bućko, J. Brzezinska-Miecznik, M. Haberko, W. Mozgawa, T. Panz, A. Pyda, J. Zarębski. *J. Europ. Ceram. Soc.* **2006**, *26*, 537.
[22] R. Barrea, C. Pérez, A. Ramos, H. Sánchez, M. Grenón. *X-Ray Spectrom.* **2003**, *32*, 387.
[23] J. B. Miecznik, K. Haberko, M. Sitarz, M. N. Bućko, B. Macherzyńska. *Ceram. Int.* **2015**, *41*, 4841.
[24] H. Wang, J. K. Lee, A. Moursi, J. J. Lannutti. *J. Biomed. Mater. Res., Part A* **2003**, *67*, 599.
[25] L. L. Hench, H. A. Paschall. *J. Biomed. Mater. Res.* **1973**, *4*, 25.
[26] Z. Abbassi, M. E. Bahrololoom, M. H. Shariat, R. Bagheri. *J. Dent. Biomater* **2015**, *2*, 1.
[27] U. M. Gross, V. Strunz. *J. Biomed. Mater. Res.* **1980**, *14*, 607.
[28] R. A. Harper, A. S. Posner. *Proc. Soc. Exp. Biol. Med.* **1966**, *122*, 137.
[29] S. Patel, S. Wei, J. Han, W. Gao. *Mater Charact* **2015**, *109*, 73.
[30] S. Pramanik, A. S. Mohd Hanif, B. Pingguan-Murphy, N. A. Abu. *Osman. Materials* **2013**, *6*, 65.
[31] T. J. Webster, C. Ergun, R. H. Doremus, R. W. Siegel, R. Bizios. *Biomaterials* **2000**, *21*, 1803.
[32] S. Madhavi, C. Ferraris, T. J. White. *J. Solid State Chem.* **2005**, *178*, 2838.
[33] S. Pramanik, B. Pingguan-Murphy, J. Cho, N. A. Abu Osman. *Sci. Rep.* **2014**, *4*, 5843.
[34] A. Slosarczyk, J. Piekarczyk. *Ceram. Int.* **1999**, *25*, 561.
[35] A. S. Rizkalla, D. W. Jones, D. B. Clarke, G. C. Hall. *J. Biomed. Mat. Res.* **1996**, *32*, 119.
[36] O. P. Filho, G. P. LaTorr, L. L. Hench. *J. Biomed. Mater. Res.* **1996**, *30*, 509.
[37] K. A. Srivastava, R. Pyare. *Int. J. Sci.Tech. Res.* **2012**, *1*, 28.
[38] J. M. Sautier, T. Kokubo, T. Ohtsuki, J. R. Nefussi, H. Boulekbache, M. Oboeuf, S. Loty, C. Loty, N. Forest. *Calcif. Tissue Int.* **1994**, *55*, 458.
[39] T. Kitsugi, T. Yamamuro, T. Nakamura, S. Higashi, K. Kakubani, K. Hyakuma, S. Ito, T. Kokubo, M. Takagi, T. Shibuya. *J. Biomed. Mater. Res.* **1986**, *20*, 1295.
[40] M. Figueiredo, J. Henriques, G. Martins, F. Guerra, F. Judas, H. Figueiredo. *J. Biomed. Mater. Res., Part B* **2010**, *92*, 409.
[41] J. C. Moreno-Pirajan, R. Gomez-Cruz, V. S. Garcia-Cuello, L. Giraldo. *J. Anal. Appl. Pyrolysis* **2010**, *89*, 122.
[42] R. A. Ramli, R. Adnan, M. Abu Bakar, S. Malik Masudi. *J. Phys. Sci.* **2011**, *22*, 25.
[43] A. Sobczak-Kupiec, D. Malina, R. Kijkowska, Z. Wzorek. *Dig. J. Nanomater. Bios.* **2012**, *7*, 385.
[44] M. Markovic, B. O. Fowler, M. S. Tung. *J. Res. Natl. Inst. Stand. Technol.* **2004**, *109*, 553.
[45] C. Lin, C. Xiao, Z. Shen. *Sci. Sintering* **2011**, *43*, 39.
[46] C. S. Ciobanu, E. Andronescu, D. Predoi. *J. Optoelectron. Adv. Mater.* **2011**, *13*, 821.
[47] H. Pirayesh. Effects of manufacturing method on surface mineralization of bioactive glasses. PhD Thesis. Edmonton: University of Alberta, Department of Chemical and Materials Engineering (**2010**).
[48] P. Sepulveda, J. R. Jones, L. L. Hench. *J. Biomed. Mater. Res., Part B* **2001**, *58*, 734.
[49] M. S. Bahniuk, H. Pirayesh, H. D. Singh, J. A. Nychka, L. D. Unsworth. *Biointerphases* **2012**, *7*, 41:1.